Journal of Solid State Chemistry 188 (2012) 32–37

Contents lists available at SciVerse ScienceDirect

Journal of Solid State Chemistry

journal homepage: www.elsevier.com/locate/jssc

Crystal chemistry of the *Pmnb* polymorph of Li_2MnSiO_4

R.J. Gummow [a,*], N. Sharma [b], V.K. Peterson [b], Y. He [a]

[a] School of Engineering and Physical Sciences, James Cook University, Townsville, Queensland 4811, Australia
[b] The Bragg Institute, Australian Nuclear Science and Technology Organization, Locked Bag 2001, Kirrawee DC NSW 2232, Australia

ARTICLE INFO

Article history:
Received 8 October 2011
Received in revised form
22 January 2012
Accepted 23 January 2012
Available online 31 January 2012

Keywords:
Neutron powder diffraction
Synchrotron X-ray powder diffraction
Infra-red spectroscopy
Polymorphism
Lithium-ion battery
Lithium manganese orthosilicate

ABSTRACT

The crystal structure of the *Pmnb* polymorph of Li_2MnSiO_4 (prepared by solid-state synthesis in argon at 900 °C) is characterized by Rietveld refinement of structural models using high resolution synchrotron X-ray and neutron powder diffraction data. The crystal structure is confirmed to be isostructural with Li_2CdSiO_4 with lattice parameters $a=6.30694(3)$, $b=10.75355(4)$, and $c=5.00863(2)$ Å, which are in good agreement with previously published data. No evidence was found for mixed lithium/manganese sites. Testing of the material as a cathode in a lithium cell shows that 1.3 lithium ions per formula unit can be extracted on the first charge cycle but very little lithium can be re-inserted. These results are compared with those of other phase-pure Li_2MnSiO_4 polymorphs.

1. Introduction

Over the last ten years, the emphasis in lithium-ion battery development has shifted from small-scale portable applications to large-scale systems. These large-scale systems are required both for electric vehicles and as storage to compensate for the variable output of renewable-energy systems. Current lithium-ion battery chemistries cannot fully meet the demands of these applications in terms of cost as well as cycle- and calendar-life. Research to find new systems and to optimize existing systems is on-going [1–3].

Expensive raw materials are a major contributor to the cost of large-scale lithium ion batteries, with the cathode as the most expensive single component. To meet the market targets for the price of these batteries it is essential to develop low-cost cathode materials [4]. The lithium transition metal orthosilicates (Li_2MSiO_4 where M=Fe, Co, or Mn), represent a new class of lithium-ion battery cathode and offer potential cost advantages because of the natural abundance of silica, iron, and manganese [5–9]. Li_2FeSiO_4 has shown promise as a cathode material [9,10], but Li_2MnSiO_4 is even more attractive. For Li_2MnSiO_4, the possibility exists for the extraction of two lithium ions per formula unit at moderate voltages, resulting in a high theoretical capacity (>300 mA h g^{-1} for the complete removal and re-insertion of two lithium ions per formula unit). Li_2MnSiO_4 has, however, so far failed to be developed as a cathode because of several limiting factors outlined below [10–14].

The practical application of Li_2MnSiO_4 as a cathode is limited by its low electronic conductivity of 5×10^{-16} S cm^{-1} at room temperature, increasing to 3×10^{-14} S cm^{-1} at 60 °C, which is 5–6 orders of magnitude smaller than that of the poorly conducting $LiFePO_4$ at room temperature [5,15]. Nanostructuring of particles and application of a conductive carbon coating on particles are both strategies employed to overcome the problem of low conductivity in $LiFePO_4$ [16]. Carbon addition is also common practice in the synthesis of Li_2MnSiO_4, resulting in composite materials with both enhanced electronic properties and improved electrochemical performance compared to carbon-free samples [10–14,17–19]. Despite efforts aimed at improving the electronic properties of Li_2MnSiO_4 by carbon addition, all reported cycling data for Li_2MnSiO_4 have shown a steady decrease in capacity with cycling. This is in contrast to cycling data for Li_2FeSiO_4, which maintains a stable discharge capacity for multiple cycles [10,20]. The failure of Li_2MnSiO_4 to cycle reversibly has been attributed to structural collapse and amorphization upon lithium extraction [5,21]. Detailed studies of the partially delithiated $Pmn2_1$ polymorph of Li_2MnSiO_4 using in-situ XRD, TEM, and NMR have clearly indicated that partial amorphization of the Li_2MnSiO_4 structure occurs upon lithium extraction [22]. This raises the question as to whether this amorphization is common to all polymorphs of Li_2MnSiO_4, or whether other polymorphs perform differently when lithium is extracted.

Phase-pure samples of Li_2MnSiO_4 are difficult to prepare as the lithium transition metal orthosilicates exhibit several different

* Corresponding author. Fax: +61 7 47816788.
E-mail address: rosalind.gummow@jcu.edu.au (R.J. Gummow).

0022-4596/$ - see front matter © 2012 Elsevier Inc. All rights reserved.
doi:10.1016/j.jssc.2012.01.051

polymorphs when synthesized under moderate conditions [8,21,23]. Arroyo-deDompablo et al. [21] have reported that there are, at least, three polymorphs of Li_2MnSiO_4 that form at ambient pressure – two orthorhombic forms (adopting $Pmn2_1$ and $Pmnb$ space group symmetries) and a monoclinic form (adopting $P2_1/n$ space group symmetry). Both the low-temperature orthorhombic forms are more stable than the monoclinic form, which can only be prepared above 900 °C [24,25]. The crystal structures of Li_2MnSiO_4 belong to the group of tetrahedral oxides with all cations tetrahedrally coordinated between distorted close-packed layers of oxygen atoms. The polymorphs can be related to the different polymorphic forms of Li_3PO_4 and differ in the orientation and connectivity of the cation tetrahedra. Structural refinements of the $Pmn2_1$ and the $P2_1/n$ forms have been reported [6,25]. In contrast, while X-ray diffraction data has been collected [21,24], no in-depth structural analysis of the $Pmnb$ form has been reported to date. All synthesized samples of this polymorph have included significant impurities, such as Li_2SiO_3, Mn_2SiO_4, MnO, and the $P2_1/n$ polymorph [21,24], preventing accurate structural determination of the $Pmnb$ form of Li_2MnSiO_4.

In this study we report the facile synthesis by solid-state techniques of essentially single-phase samples of the $Pmnb$ polymorph of Li_2MnSiO_4 and its crystal-structure determined using synchrotron X-ray powder diffraction (SXRPD) and neutron powder diffraction (NPD) data. Morphological and FTIR spectroscopy data, as well as galvanostatic cell-cycling performance in lithium cells, are also reported.

2. Experimental

Samples of Li_2MnSiO_4 were synthesized by a solid-state route. Stoichiometric quantities of LiOH (Sigma–Aldrich, $>98\%$), $MnCO_3$ (Sigma–Aldrich, $>99.9\%$), SiO_2 (fumed, Sigma–Aldrich, 0.007 μm), together with 20 mol% adipic acid, were milled with dry hexane in a vibratory ball mill for 1 h. The mixed powders were heated at 1 °C per min to 450 °C for 10 h under dynamic vacuum to decompose the precursors. The resulting fine, dark brown powder was ground in a mortar and pestle and then heated to 700 °C for 10 h in argon in a tube furnace to prevent oxidation of the Mn^{2+}. To complete the reaction, the sample was heated to 900 °C for a further 10 h in argon and allowed to cool to room temperature in the furnace. Sample powders were stored in an argon glovebox.

The synthesized powders were initially characterized by conventional X-ray powder diffraction (XRPD) using a Siemens D5000 and a Panalytical X'pert Pro X-ray diffractometer with Cu-K_α radiation. Additional high-resolution SXRPD data were collected on the Powder Diffraction beamline (10-BM-1) [26] at the Australian Synchrotron using a wavelength (λ) of 0.82599(2) Å, determined using the NIST 660a LaB_6 standard reference material. Powder samples were packed and sealed in 0.5 mm glass capillaries in an argon glovebox and data were collected for 6 min at ambient temperature using Debye–Scherrer geometry. Neutron powder diffraction (NPD) data were collected using the high-resolution powder diffractometer, ECHIDNA, at the Open Pool Australian Light-water (OPAL) reactor facility at the Australian Nuclear Science and Technology Organisation (ANSTO) [27]. Data were collected at $\lambda = 1.62285(2)$ Å for 9 h in the 2θ range $14 \le 2\theta \le 154°$, with the wavelength determined using the NIST Al_2O_3 SRM 676. Samples were sealed in 6 mm diameter vanadium cans with indium gaskets in an argon glovebox and data were collected at ambient temperature. Rietveld refinements were carried out using the GSAS [28] software suite with the EXPGUI [29] software interface. The SXRD and NPD datasets were initially refined separately. Finally, a combined refinement of both the SXRD and NPD datasets was performed. Atomic parameters for the elements in the starting model of the combined refinement were derived from the single dataset refinements, using the results from the dataset that provided the better contrast for each element relative to others. Using this approach, parameters for manganese and silicon were taken from the SXRPD data-derived model and parameters for the lithium and oxygen were taken from the NPD data-derived model.

Particle morphology was determined by analysis of scanning-electron microscope images obtained with a JEOL JSM-5410LV instrument. Lithium and manganese content was determined by inductively coupled plasma-atomic emission spectrometry (ICP-AES) using a Varian Liberty Series II instrument. Samples were digested in hydrofluoric acid prior to analysis. Silicon is lost in the digestion process and therefore could not be analyzed.

Energy-dispersive spectroscopy (EDS) was performed on carbon-coated powder samples using an electron-probe micro analyzer (EPMA) to determine the manganese to silicon ratio of the product phases. Averages were taken of six measurements at different positions in the sample. Elements with low atomic mass cannot accurately be analyzed on this instrument so it was not possible to accurately determine lithium or oxygen contents.

FTIR spectra were collected on powder samples in transmission mode between 700 and 1400 cm^{-1} using the diamond ATR on a Perkin–Elmer FTIR spectrometer (see the Supporting Information).

To prepare electrodes for electrochemical characterization the sample powder was ball-milled with Super C-65 carbon (Timcal) in a vibratory ball-mill for 1 h. The resulting powder was mixed with polyvinylidene difluoride (PVDF, Sigma–Aldrich) dissolved in n-methyl pyrrolidenone (NMP, anhydrous, 99.5%, Sigma–Aldrich) in a ratio of 74:13:13. Cathodes were formed by coating the resulting slurry onto aluminum foil current collectors, followed by drying in vacuum for 10 h at 120 °C and pressing with a hydraulic press to 15 MPa. Typical cathode masses were 1–2 mg with a surface area of 1.2 cm^2. Swagelok-type electrochemical test-cells were assembled in an argon glovebox. The electrolyte used was a solution of lithium hexafluorophosphate (battery grade, $>99.9\%$, Aldrich) in a 1:1 mixture by volume of ethylene carbonate and dimethyl carbonate (99%, Sigma–Aldrich). The anode consisted of a 12 mm diameter disk of 0.7 mm thick lithium metal foil. The anode and cathode were separated by two disks of microporous polypropylene separator film (Celgard) saturated with the electrolyte solution. Assembled cells were cycled galvanostatically using a battery analyzer (MTI Corporation).

3. Results and discussion

3.1. Structural determination

XRPD data for the samples formed at 700 °C and 900 °C are shown in Fig. 1(b) and (c), respectively, together with a simulated XRPD pattern of the $Pmn2_1$ form of Li_2MnSiO_4 using the structural model of Dominko et al. [6] (Fig. 1(a)). We speculate that the presence of the carbon-containing adipic acid in the reaction mixture inhibits the formation of Li_2MnSiO_4 at 700 °C in argon; after 10 h peaks attributed to both Li_2SiO_3 and MnO remain (Fig. 1(b)). The disappearance of these impurity peaks on further heating to 900 °C for 10 h (Fig. 1(c)) indicates that the reaction approaches completion at this temperature. The product was a dark gray color and the relatively sharp diffraction peaks indicate that a crystalline product formed at the relatively high temperature of 900 °C. Notably, the XRPD data of the material obtained after heating to 900 °C (Fig. 1(c)) contains peaks that are not present in the $Pmn2_1$ model for Li_2MnSiO_4 (Fig. 1(a)), but

conforms to the expected pattern for the *Pmnb* form as described by Arroyo-deDompablo et al. [21] and Mali et al. [24]. In the study of Belharouak et al. [11], it was reported that Li_2MnSiO_4 samples heated above 700 °C contained Li_2SiO_3 and Mn_2SiO_4 impurities; 700 °C was found to be the optimal temperature for the synthesis of Li_2MnSiO_4 with the $Pmn2_1$ structure. In the present study heating the sample above 700 °C does not result in the formation of impurities but leads to the formation of the phase-pure *Pmnb* form of Li_2MnSiO_4. This sample represents the purest *Pmnb* form of Li_2MnSiO_4 that has been reported, a material that has proved difficult to synthesize without significant impurities in the past, and the crystallographic structure was studied further using high resolution SXRPD and NPD.

The Li_2CdSiO_4–type [30] structure proposed by Arroyo-deDompablo et al. [21] and Mali et al. [24] for the *Pmnb* form of Li_2MnSiO_4, was used as a starting model with silicon, lithium, and manganese each occupying individual atomic sites without any cation mixing. No evidence was found for Li_2SiO_3 and Mn_2SiO_4 impurities or other polymorphs of Li_2MnSiO_4 in the sample. A few small reflections in the SXRPD data were accounted for with the inclusion of MnO as a minor impurity phase ($<1\%$). Permutations of the ideal model, such as lithium-ion vacancies and cation mixing on lithium and/or manganese sites, were tested but were not found to describe the data (i.e., did not result in statistically significant improvements of the fit of the model to the data).

The structural model and permutations tested against the SXRPD data were again tested against the NPD data. The Lobanov and Alte da Veiga absorption correction [28,31] was applied in the Rietveld model to account for absorption of neutrons by the sample, which was significant as a consequence of the relatively large neutron absorption cross-section of lithium (63.632 barn at $\lambda=1.62285(2)$ Å) [32]. The ideal model, containing no cation mixing, proved to be the best fit to the NPD data. Model permutations such as lithium-ion vacancies and mixed sites were tested and again were found not to describe the data.

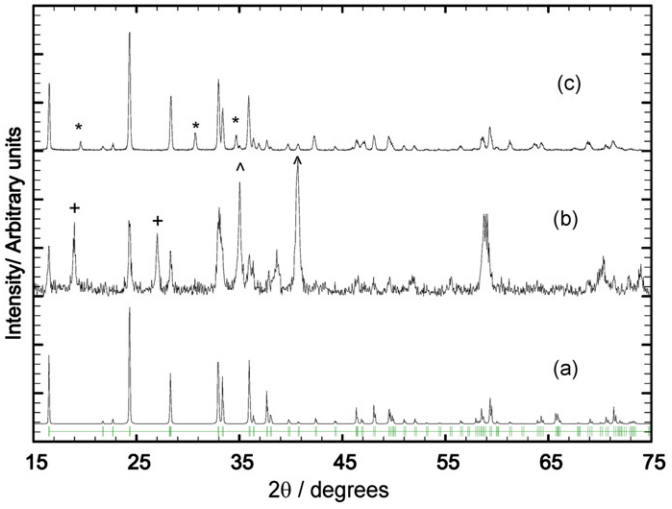

Fig. 1. (a) Calculated XRPD pattern for the $Pmn2_1$ polymorph of Li_2MnSiO_4 (vertical lines indicate peak positions) and collected patterns of Li_2MnSiO_4 synthesized at (b) 700 °C and (c) 900 °C where reflections marked with (+) are from Li_2SiO_3, (^) are from MnO and (*) are peaks unaccounted for with the $Pmn2_1$ structural model.

Rietveld refinement of the structural model was performed using both SXRPD and NPD datasets simultaneously, referred to as a combined refinement [33–35]. The refined lattice parameters obtained from the combined refinement are $a=6.30694(3)$ Å, $b=10.75355(4)$ Å, and $c=5.00863(2)$ Å, which are closer to the lattice constants reported by Arroyo-deDompablo et al. of $a=6.30814(13)$ Å, $b=10.75946(22)$ Å and $c=5.00909(10)$ Å for the *Pmnb* phase [21], than to those reported by Mali et al. of $a=6.3148(1)$ Å, $b=10.7742(5)$ Å, and $c=5.0138(2)$ Å [24]. The manganese to silicon ratio of the sample, analyzed using EDS, was found to be 0.9(1):1.0 and the lithium to manganese ratio obtained from the ICP-AAS analysis was 2:0.95(3). These results are in agreement with the nominal stoichiometry of Li_2MnSiO_4. The final structural model (Table 1), with lithium, manganese, and silicon ions fully occupying individual tetrahedral sites and no cation mixing is obtained from combined refinements with 45 variables with figures of merit that include the profile factor (R_p)=2.74%, the weighted-profile factor (wR_p)=3.70%, and the goodness-of-fit term (χ^2)=1.86, and Bragg *R*-factors (R_F^2) of 9.31% and 8.73% for the NPD and SXRPD reflection lists, respectively (Figs. 2(a), (b) and 3). Bond-valence sums (BVS) [35], bond lengths, and bond angles for the refined structural model were physically reasonable (Tables 1 and 2).

The structural model obtained in this study confirms the proposed Li_2CdSiO_4-type structure for the *Pmnb* polymorph of Li_2MnSiO_4 (Fig. 4(a)) [21,24]. The structure features two-dimensional "layers" of alternating, corner-sharing silicon and manganese tetrahedra in the (0 1 0) plane linked along the [0 1 0] direction by double-chains of lithium tetrahedra. The SiO_4 and MnO_4 tetrahedra share corners with the lithium tetrahedra. The two chains of Li tetrahedra share faces in the [0 1 0] direction. There is no face-sharing between the MnO_4 tetrahedra and either the SiO_4 or LiO_4 tetrahedra. It should be noted that this structure is different from that of the recently reported *Pmnb* polymorph of Li_2FeSiO_4 formed at 900 °C, in which edge-sharing of the LiO_4 and FeO_4/CoO_4 tetrahedra occurs [36,37].

The average Si–O and Li–O bond lengths are 1.644(3) Å and 1.961(9) Å, respectively (Table 2). These bond lengths are in agreement with the expected distances of 1.64 Å and 1.97 Å for Si–O and Li–O, respectively, based on their expected ionic sizes in tetrahedral coordination [38,39]. The average Mn–O bond length of 2.079(3) Å is significantly larger than the expected bond length of 2.04 Å, based on ionic size, but is in reasonable agreement with the average value of 2.0910 Å predicted by the computational model of Arroyo-deDompablo et al. [21] for the *Pmnb* structure. This indicates that the manganese tetrahedra are distorted, which

Table 1
Refined crystallographic parameters for Li2MnSiO4, space group *Pmnb* using combined SXRPD and NPD data, with $a=6.306938(25)$ Å, $b=10.75355(4)$ Å, and $c=5.008629(23)$ Å, with combined parameters $R_p=2.74\%$, $wR_p=3.70\%$, and $\chi^2=1.86$, and R_F^2 (NPD)=9.31%, and R_F^2 (SXRPD)=8.73% for 45 variables.

Atom	Wyckoff	*x*	*Y*	*z*	Site occupancy factor	Isotropic atomic displacement parameter (× 100)/Å^2	Bond valence sum
Li(1)	8d	0.5077(8)	0.9129(4)	0.3133(10)	1	2.55(10)	1.06
Mn(1)	4c	0.25	0.1653(1)	0.1942(2)	1	0.78(1)	1.69
Si(1)	4c	0.25	0.3386(1)	0.6790(3)	1	1.39(33)	3.80
O(1)	4c	0.25	0.3433(2)	0.3417(4)	1	1.19(5)	1.82
O(2)	8d	0.0366(2)	0.0907(1)	0.2848(3)	1	0.78(4)	1.95
O(3)	4c	0.25	0.1926(2)	0.7574(4)	1	0.61(5)	1.87

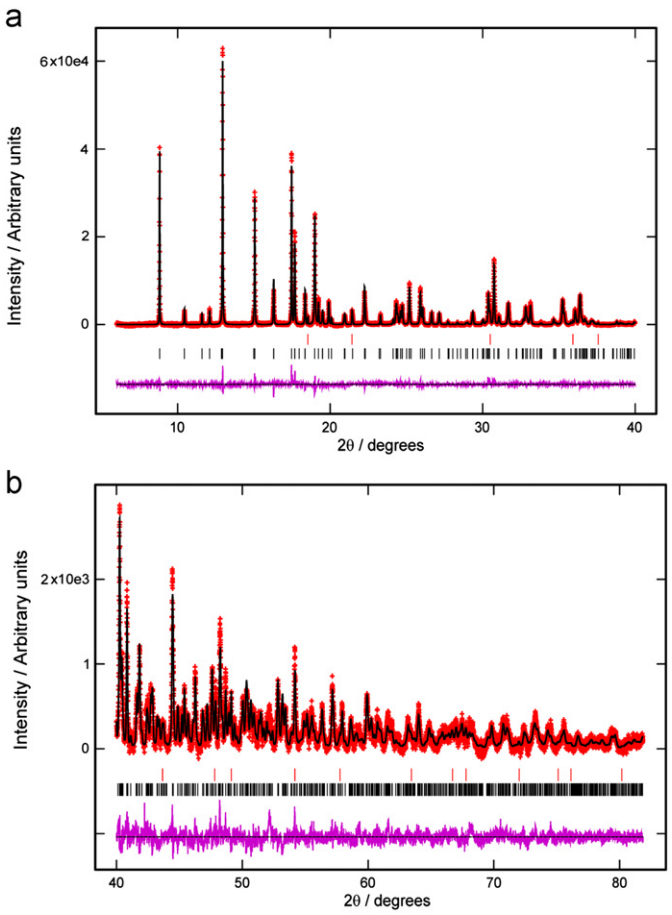

Fig. 2. The Rietveld refinement plot using the Li_2MnSiO_4 *Pmnb* model and SXRPD data in the (a) $5 \leq 2\theta \leq 40^\circ$ and (b) $40 \leq 2\theta \leq 80^\circ$ regions. Data are shown as crosses, the calculated Rietveld model as a line through the data, and the difference between the data and the model as the line below the data. The reflection markers for Li_2MnSiO_4 (lower markers) and MnO (upper markers) are shown as vertical lines.

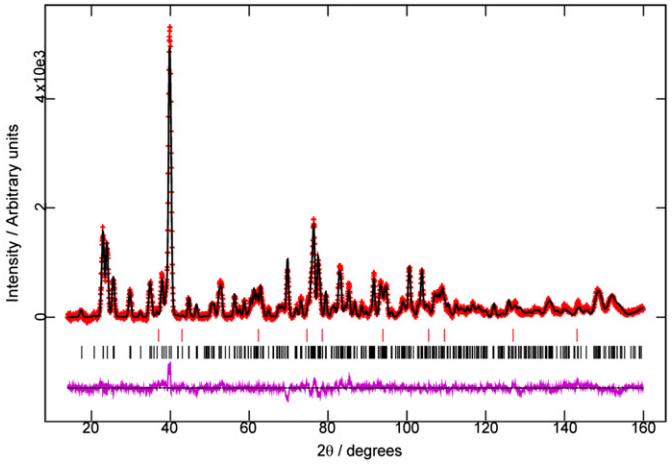

Fig. 3. The Rietveld refinement plot using the Li_2MnSiO_4 *Pmnb* model and NPD data. Data are shown as crosses, the calculated Rietveld model as a line through the data, and the difference between the data and the model as the line below the data. The reflection markers for Li_2MnSiO_4 (lower markers) and MnO (upper markers) are shown as vertical lines.

is confirmed by the large distribution of O–Mn–O bond angles. This finding is in agreement with the published data for Li_2CdSiO_4 which shows distorted Cd tetrahedra [30].

BVS (Table 1) show that all atoms (with the exception of lithium) are underbonded. In particular, the BVS sum for manganese is 15.5% less than the expected value, which is consistent with the distorted manganese tetrahedra (Table 2). The BVS for the other atoms, although less than the expected values, are within the acceptable range of values considering the approximate nature of BVS calculations.

Complete delithiation of Li_2MnSiO_4 with *Pmnb* symmetry (Fig. 4(b)) would result in $MnSiO_4$ layers disconnected from each other, causing lattice expansion along the *y*-direction as a consequence of the electrostatic repulsion of the oxygen anions in adjacent layers. This delithiated state is therefore unlikely to occur in practice. It is more likely that delithiation of Li_2MnSiO_4 with *Pmnb* symmetry would result in a lattice re-arrangement (as demonstrated for Li_2FeSiO_4) or structural collapse and amorphization (as found for the $Pmn2_1$ polymorph of Li_2MnSiO_4) [5,13,22,40]. A driver for structural change is the instability of Mn^{3+} and Mn^{4+} in tetrahedral coordination. Mn^{3+} is typically found in distorted octahedral or square-pyramidal coordination while Mn^{4+} is usually found in octahedral coordination. This implies that oxidizing Mn^{2+} while maintaining tetrahedral coordination is likely to be difficult [25]. The presence of Mn^{3+} cations in delithiated Li_2MnSiO_4 may also result in a dynamic Jahn–Teller distortion of the lattice, which has been shown to be a significant factor in the capacity fade of other Mn^{3+}-containing cathode materials such as $LiMn_2O_4$ spinels [41].

3.2. Morphology

SEM analysis of the material shows that smaller particles are sintered together to form larger, irregular agglomerates of up to 50 μm, consistent with the relatively high temperature of synthesis (900 °C, Fig. 5). Despite the presence of the carbonaceous additive (adipic acid), the sintering process is not inhibited at this high temperature.

3.3. Electrochemistry

Fig. 6 shows the galvanostatic charge and discharge curves for the first cycle for a Li/Li_2MnSiO_4 (*Pmnb* polymorph) cell at ambient temperature with a current rate of 20 mAg^{-1} and voltage limits of 4.9 and 2.5 V, respectively. The first charge cycle shows a steady increase in voltage with charge and a capacity of 230 mA h g^{-1}, corresponding to the extraction of 1.3 lithium per formula unit. Lithium cannot be re-inserted in large quantities on the subsequent discharge (20 mA h g^{-1}, corresponding to 0.1 lithium per formula unit).

The poor electrochemical performance may be ascribed to two factors. First, it should be noted that the morphology of this sample (Fig. 5), prepared by solid-state synthesis, is not optimal for electrochemical performance. Large, poorly-conducting particles result in large polarization and it is possible that some of the capacity observed on charge can be attributed to irreversible reactions, for example, electrolyte decomposition, occurring at the high voltages reached and not exclusively to lithium extraction. Since the *Pmnb* polymorph of Li_2MnSiO_4 can be readily formed in the solid state at 900 °C, alternative synthesis routes e.g., sol–gel or hydrothermal synthesis that typically generate fine particles with a carbon coating, are also expected to yield this polymorph at calcination temperatures above 700 °C. Fine, carbon-coated powders would show reduced polarization on charge enabling the extraction of lithium at lower voltages and preventing unwanted side-reactions. Second, it is likely that, as in the case of the $Pmn2_1$ polymorph, the extraction of lithium during the first charge cycle results in a structural re-arrangement or

Table 2
Selected bond lengths (Å) and bond angles (°) of the *Pmnb* phase of Li_2MnSiO_4.

Bond	Length (Å)	Bond	Length (Å)	Bond	Length (Å)
Li–O(1)	1.950(5)	Mn–O(1)	2.051(2)	Si–O(1)	1.690(2)
Li–O(2)	1.926(4)	Mn–O(2)	2.029(1)	Si–O(2)	1.633(1)
Li–O(2)	2.033(4)	Mn–O(2)	2.029(1)	Si–O(2)	1.633(1)
Li–O(3)	1.936(5)	Mn–O(3)	2.207(2)	Si–O(3)	1.618(2)
Average	1.961(9)	Average	2.079(3)	Average	1.644(3)
Angle	(°)	**Angle**	(°)	**Angle**	(°)
O(1)–Li–O(2)	115.52(26)	O(1)–Mn–O(2)	106.77(4)	O(1)–Si–O(2)	108.08(8)
O(1)–Li–O(2)	105.78(22)	O(1)–Mn–O(2)	106.77(4)	O(1)–Si–O(2)	108.08(8)
O(1)–Li–O(3)	111.10(20)	O(2)–Mn–O(2)	125.97(8)	O(1)–Si–O(3)	105.76(13)
O(2)–Li–O(2)	96.06(21)			O(2)–Si–O(2)	110.89(12)
O(2)–Li–O(3)	119.56(25)			O(2)–Si–O(3)	111.88(7)
O(2)–Li–O(3)	106.14(23)			O(2)–Si–O(3)	111.88(7)

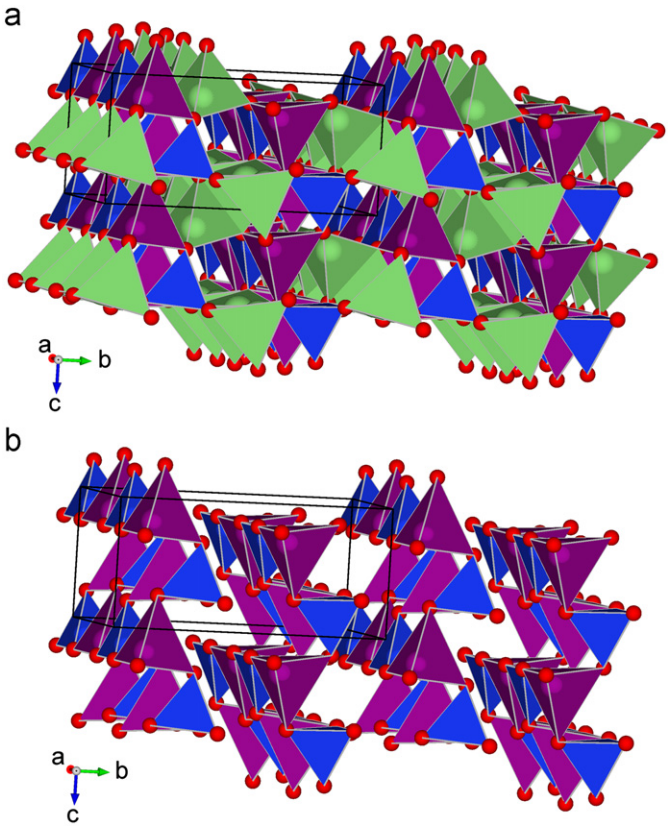

Fig. 4. The crystal structure of (a) the *Pmnb* form of Li_2MnSiO_4 and (b) the hypothetical structure of the fully delithiated $MnSiO_4$ with SiO_4 shown in blue, LiO_4 in green, and MnO_4 in purple. The central ions in the tetrahedra are shown to indicate the tetrahedral orientation. Crystal axes are shown inset at the bottom left and indicate orientation.

amorphization of the lattice which limits lithium re-insertion on the subsequent discharge cycle [5,13,22].

4. Conclusion

In this study we have prepared the *Pmnb* polymorph of Li_2MnSiO_4 without significant impurities. Rietveld refinement of a structural model using a combination of high resolution SXRPD and NPD data shows that the sample is isostructural with Li_2CdSiO_4 with $a=6.30694(3)$ Å, $b=10.75355(4)$ Å, and $c=5.00863(2)$ Å, confirming the previously proposed structure [21,24]. Bond lengths, angles, and BVS from this model are physically realistic, where the manganese tetrahedra are found to be distorted. Electrochemical results show poor galvanostatic cycling performance. Alternative synthesis routes aimed at improving the electrochemical performance of this polymorph will be explored in future work.

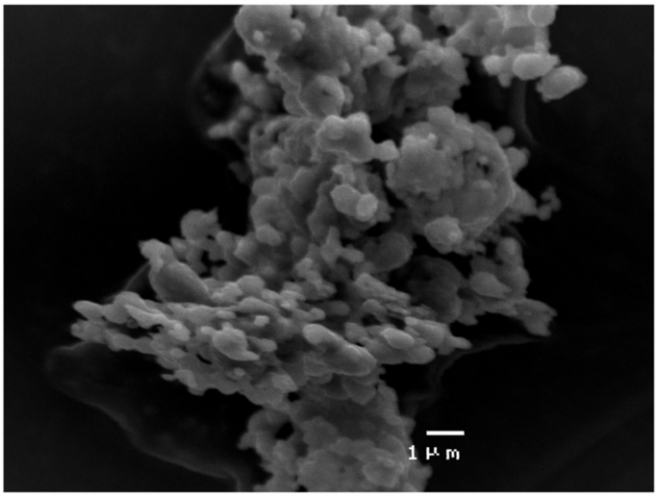

Fig. 5. SEM micrograph of the as-prepared *Pmnb* polymorph of Li_2MnSiO_4.

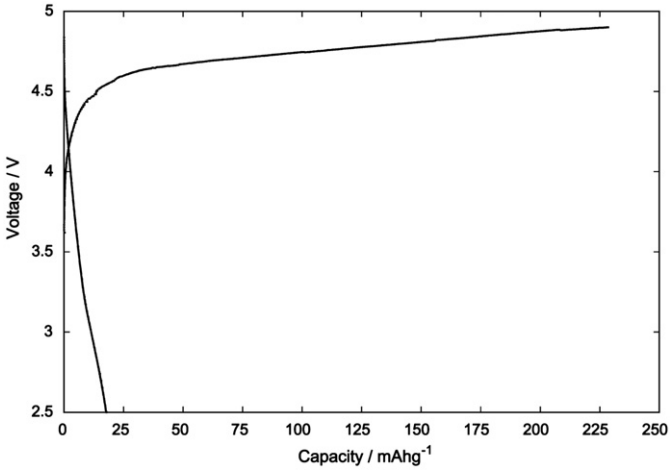

Fig. 6. Galvanostatic cycling curves for the first charge and discharge cycles of a Li/Li_2MnSiO_4 (*Pmnb* form) cell cycled at a current rate of 20 mA g^{-1} between voltage limits of 2.5 and 4.8 V.

Acknowledgments

Dr Jen Whan and Dr Shane Askew of the Advanced Analytical Centre, JCU, are thanked for technical assistance with the XRPD, EDS, and SEM data acquisition. Dr Yi Hu (AAC) is thanked for the ICP-MS data acquisition.

The Faculty of Science and Engineering (JCU) is thanked for financial support for this project by means of a New Staff Grant for Dr R. J. Gummow.

This research was undertaken on the Powder Diffraction beamline at the Australian Synchrotron, Victoria, Australia and we would like to thank Dr. Qinfen Gu for his assistance.

Dr R. J. Gummow would like to thank AINSE for travel and accommodation support to the Bragg Institute under grant number P2172.

Dr R. J. Gummow would like to thank Timcal for the supply of Super C-65 carbon.

Appendix A. Supplementary information

Supplementary data associated with this article can be found in the online version at doi:10.1016/j.jssc.2012.01.051.

References

[1] Z.G. Yang, J. Liu, S. Baskaran, C.H. Imhoff, J.D. Holladay, JOM-J. Min. Met. Mat. S. 62 (2010) 14–23.
[2] T. Xu, W. Wang, M.L. Gordin, D.H. Wang, D.W. Choi, JOM-J. Min. Met. Mat. S. 62 (2010) 24–30.
[3] A. Manthiram, J. Phys. Chem. 2 (2011) 176–184.
[4] C. Daniel, JOM-J. Min. Met. Mat. S. 60 (2008) 43–48.
[5] R. Dominko, J. Power, Sources 184 (2008) 462–468.
[6] R. Dominko, M. Bele, M. Gaberscek, A. Meden, M. Remskar, J. Jamnik, Electrochem. Commun. 8 (2006) 217–222.
[7] R. Dominko, M. Bele, A. Kokalj, M. Gaberscek, J. Jamnik, J. Power Sources 174 (2007) 457–461.
[8] C. Lyness, B. Delobel, A.R. Armstrong, P.G. Bruce, Chem. Commun. (2007) 4890–4892.
[9] A. Nyten, A. Abouimrane, M. Armand, T. Gustafsson, J.O. Thomas, Electrochem. Commun. 7 (2005) 156–160.
[10] C. Deng, S. Zhang, B.L. Fu, S.Y. Yang, L. Ma, Mater. Chem.Phys. 120 (2010) 14–17.
[11] I. Belharouak, A. Abouimrane, K. Amine, J. Phys. Chem. C 113 (2009) 20733–20737.
[12] W.G. Liu, Y.H. Xu, R. Yang, J. Alloys Compd. 480 (2009) L1–L4.
[13] W.G. Liu, Y.H. Xu, R. Yang, Rare Met. 29 (2010) 511–514.
[14] W.G. Liu, Y.H. Xu, R. Yang, M. Hojamberdiev, Z.B. Zhou, J. Inorg. Mater. 25 (2010) 327–331.
[15] V. Srinivasan, J. Newman, J. Electrochem. Soc. 151 (2004) A1517–A1529.
[16] J.D. Wilcox, M.M. Doeff, M. Marcinek, R. Kostecki, J. Electrochem. Soc. 154 (2007) A389–A395.
[17] A. Manthiram, T. Muraliganth, K.R. Stroukoff, Chem. Mater. 22 (2010) 5754–5761.
[18] V. Aravindan, K. Karthikeyan, S. Ravi, S. Amaresh, W.S. Kim, Y.S. Lee, J. Mater. Chem. 20 (2010) 7340–7343.
[19] K. Karthikeyan, V. Aravindan, S.B. Lee, I.C. Jang, H.H. Lim, G.J. Park, M. Yoshio, Y.S. Lee, J. Power Sources 195 (2010) 3761–3764.
[20] D. Lv, W. Wen, X. Huang, J. Bai, J. Mi, S. Wu, Y. Yang, J. Mater. Chem. 21 (2011) 9506–9512.
[21] M.E. Arroyo-deDompablo, R. Dominko, J.M. Gallardo-Amores, L. Dupont, G. Mali, H. Ehrenberg, J. Jamnik, E. Moran, Chem. Mater. 20 (2008) 5574–5584.
[22] A. Kokalj, R. Dominko, G. Mali, A. Meden, M. Gaberscek, J. Jamnik, Chem. Mater. 19 (2007) 3633–3640.
[23] A.R. Armstrong, C. Lyness, M. Menetrier, P.G. Bruce, Chem. Mater. 22 (2010) 1892–1900.
[24] G. Mali, A. Meden, R. Dominko, Chem. Commun. 46 (2010) 3306–3308.
[25] V.V. Politaev, A.A. Petrenko, V.B. Nalbandyan, B.S. Medvedev, E.S. Shvetsova, J. Solid State Chem. 180 (2007) 1045–1050.
[26] K.S. Wallwork, B.J. Kennedy, D. Wang, AIP Conf. Proc. (2007) 879.
[27] K.D. Liss, B. Hunter, M. Hagen, T. Noakes, S. Kennedy, Physica B 385-86 (2006) 1010–1012.
[28] A.C. Larson, R.B.V. Dreele, Los Alamos National Laboratory Report LAUR (1994) pp. 86–748.
[29] B.H. Toby, J. Appl. Crystallogr. 34 (2001) 210–213.
[30] C. Riekel, Acta Crystallogr., B 33 (1977) 2656–2657.
[31] N.N. Lobanov, L.A.d. Veiga, Sixth European Powder Diffraction Conference August pp. 22–25 (1998).
[32] V.F. Sears, Neutron News 3 (1992) 29.
[33] N. Sharma, R.L. Withers, K.S. Knight, C.D. Ling, J. Solid State Chem. 182 (2009) 2468–2474.
[34] N. Sharma, R.B. Macquart, M.M. Avdeev, M. Christensen, G.I. McIntyre, Y.-S. Chen, C.D. Ling, Acta Crystallogr., B 66 (2010) 165–172.
[35] R.J. Gummow, N. Sharma, V.K. Peterson, Y. He, J. Power Sources (2011). doi:10.1016/j.jpowsour.2011.09.013.
[36] A. Boulineau, C. Sirisopanaporn, R. Dominko, A.R. Armstrong, P.G. Bruce, C. Masquelier, Dalton Trans. 39 (2010) 6310–6316.
[37] C. Sirisopanaporn, A. Boulineau, D. Hanzel, R. Dominko, B. Budic, A.R. Armstrong, P.G. Bruce, C. Masquelier, Inorg. Chem. 49 (2010) 7446–7451.
[38] R.D. Shannon, C.T. Prewitt, J. Inorg. Nucl. Chem 32 (1970) 1427–1441.
[39] R.D. Shannon, C.T. Prewitt, Acta Crystallogr., B 25 (1969) 925.
[40] A.R. Armstrong, N. Kuganathan, M.S. Islam, P.G. Bruce, J. Am. Chem. Soc. 133 (2011) 13031–13035.
[41] R.J. Gummow, A. De Kock, M.M. Thackeray, Solid State Ionics 69 (1994) 59–67.